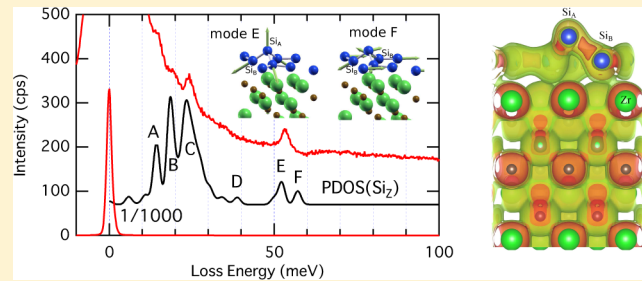


Silicene on Zirconium Carbide (111)

Takashi Aizawa,* Shigeru Suehara, and Shigeki Otani

National Institute for Materials Science, 1-1 Namiki, Tsukuba, Ibaraki 305-0044, Japan

ABSTRACT: A silicon monatomic layer (i.e., silicene) forms an ordered phase on the surface of ZrC(111) in the 2×2 periodicity of the substrate. For the first time, phonon dispersion relations were measured using high-resolution electron energy loss spectroscopy (HREELS) on a silicene sheet. The atomic structure and phonon dispersions were calculated using ab initio density functional theory. Nearly all the surface-localized phonon modes were well reproduced, and especially the dipole-active phonon modes well corresponded to the peaks in the specular HREEL spectrum. The optimized atomic structure was a distorted silicene on the Zr-terminated ZrC(111), in which the $\sqrt{3} \times \sqrt{3}$ unit cell of Si₆ coincides with the 2×2 unit of the substrate ZrC(111). In the unit cell, one Si atom sits on the on-top site of the Zr substrate; three atoms are placed at the bridge sites of the substrate; and two other atoms are on the 3-fold hollow sites above the third layer (C) and above the fourth layer (Zr). This structure is prevalent on several metal substrates.



INTRODUCTION

The two-dimensional honeycomb lattice of Si, which is an isomorph of graphene, has been named “silicene”. A recent understanding of silicene on Ag(111) has ignited increasing attention because of its promising versatilities.¹ The atomic structures,^{2–9} electronic structures,^{10–14} and lattice vibrations^{15–17} of the most extensively studied system, Si/Ag(111), have been reported. Studies on silicene formation on other metallic substrates are being published.^{18,19}

Lattice dynamics of monolayer material provides information about the material properties. In fact, measurements of graphene phonon structure provided important insight on the interaction between graphene and the substrate.^{20,21} As for silicene, phonons of a free-standing silicene were theoretically studied by several groups.^{22–25} However, except for Si on Ag(111), only a few studies on the lattice dynamics of a silicene layer on other substrates have been reported either experimentally or theoretically.

Transition-metal carbides (TMCs) and diborides belong to a group of compounds having high melting point, high hardness, high stability to oxidation, and high electric conductivity. They have promising applications to high-temperature ceramics and are highly stable substrates for film growth. ZrB₂(0001) has lattice and thermal expansion parameters similar to those of GaN, resulting in high quality epitaxy.^{26–28} On TMC(111) surfaces, GaN epitaxy can occur,²⁹ but lattice constant matching is critical. Fleurence et al. reported silicene formation on the surface of ZrB₂(0001).¹⁹ They interpreted the structure of the system as a 2×2 overlayer. As per the substrate lattice constant (316.8 pm) of ZrB₂(0001), the silicene lattice constant must be 365.8 pm, which is very small compared to the calculated value of 383–389 pm for the free-standing buckled silicene.^{22–24} Their scanning tunneling microscope (STM) image exhibited a

stripe-domain structure,¹⁹ and their low-energy electron diffraction (LEED) pattern³⁰ exhibited splittings on the 1/2-order spots, characteristic of an incommensurate structure. Conversely, ZrC(111) has a large in-plane lattice parameter a (332 pm), for which the ratio $2a/\sqrt{3} = 383$ pm fits the silicene.

Here we have produced a monatomic Si layer on ZrC(111), which ordered in the 2×2 unit cell similar to Si/ZrB₂(0001). We have performed phonon dispersion measurements of this system using high-resolution electron energy loss spectroscopy (HREELS). Ab initio density functional theory (DFT) calculation revealed a stable atomic structure that was identified as distorted silicene, the lattice dynamics of which well matched the measured phonons.

METHODS

Experiment. The experiment was performed in a two-chamber ultrahigh vacuum (UHV) system for surface analysis. One chamber was made of a high permeability alloy (PC permalloy) for HREELS, which was evacuated with a sputter ion pump (400 L/s) and a nonevaporable getter pump (1300 L/s), achieving an UHV of 7×10^{-10} to 2×10^{-9} Pa. The residual magnetic field in the chamber was less than 1/10 of the geomagnetic field. The chamber was equipped with a HREEL spectrometer (Delta 0.5, SPECS GmbH), and LEED optics for azimuth setting were used. HREELS was operated with a resolution of 1.5–2 meV in order to obtain a reasonable signal-to-noise ratio. The other chamber was a conventional stainless-steel UHV chamber with a base pressure of 3×10^{-9} to 1×10^{-8} Pa for sample preparation, evacuated with a turbomo-

Received: June 5, 2014

Revised: September 13, 2014

Published: September 15, 2014

lecular pump (300 L/s). A reflection high-energy electron diffraction (RHEED) system, a cylindrical mirror analyzer for Auger electron spectroscopy (AES), a silicon evaporator, and a load lock system were mounted on this chamber. The RHEED gun was used as the excitation source in AES measurement, in which the 15 keV electron beam was impinged on the sample at approximately 70° from the surface normal. A transfer tube was permitted to move the sample in UHV between HREELS and preparation chambers.

A ZrC(111) film grown epitaxially on an NbC(111) single-crystal surface was used as the substrate. The NbC single crystal was grown using the radio frequency-heated floating zone method. A sample disk (7–9 mm in diameter and 1–1.5 mm in thickness) of (111) faces was cut from the rod using spark erosion after X-ray Laue orientation. One face of the sample was polished to a mirror finish using B_4C powder and diamond pastes. After ultrasonic washing in acetone, the sample was introduced in the vacuum and heated with electron bombardment from the backside. The sample temperature was monitored using optical pyrometers without calibration. ZrC was deposited by using an electron-beam-heated evaporator (EFM3, Omicron NanoTechnology GmbH). A sintered ZrC rod was used as the evaporation source.

Si was evaporated from a direct-current-heated (12–13 Å) Si wafer ($20 \times 4 \times 0.5$ mm³) placed ahead of the substrate at approximately 30 mm away. The deposition rate was approximately 5×10^{17} m⁻² s⁻¹, which corresponded to 0.03 Si(111) double layers per second.

In the HREELS measurement, the incidence angle θ_{in} was fixed at 75° from the surface normal, and the detection angle was varied. In specular conditions, i.e., detection angle θ_{out} equal to θ_{in} , the dipole-active phonon modes were efficiently observed.³¹ By varying θ_{out} , the excited phonon wave vector parallel to the surface was scanned to obtain the surface phonon dispersion relations. A loss peak in the spectrum was fitted to a Gaussian function with a constant background to determine the loss energy. Only peaks recognizable by eyes were taken, and no peak separation technique was applied.

Calculation. First-principles DFT calculations were performed using the Quantum ESPRESSO code.³² The exchange correlation was implemented with the Perdew–Burke–Ernzerhof (PBE) functional.³³ When the GBRV ultrasoft pseudopotentials were used,³⁴ self-consistent electronic ground-state calculations were iterated until the error reached $<10^{-10}$ Ry/atom. Structure optimizations with no symmetry assumption were performed to achieve residual stress and forces of less than 0.5 kbar and 0.1 mRy/bohr, respectively. Phonon dispersion calculations were performed using the density-functional perturbation theory.³⁵ The surface was modeled with a slab supercell construction divided by a vacuum layer thicker than 1 nm (1.2–1.4 nm). The parameters listed in Table 1 are those obtained from the tests of the energy convergence with the slab thickness, cutoff energy, and *k*-point number in the Monkhorst–Pack scheme.

The calculated crystal and electronic structures were visualized using the XCrySDEN³⁶ and VESTA³⁷ programs. The calculations were performed on workstations (Xeon 2.8 GHz, 96 cores) and on a numerical materials simulator (SGI Co. Ltd.) located at our institute.

■ ZRC(111) SUBSTRATE

ZrC(111) Film Growth. The NbC(111) was cleaned with degas heating at 1500 K and following several flash heatings up

Table 1. Parameters Used in the Calculation^a

model	thickness	cutoff (Ry)	<i>k</i> -points
bulk ZrC		30	$12 \times 12 \times 12$
1 × 1 slab A	$7Zr + 6C$	30	$12 \times 12 \times 1$
2 × 2 slab B	$1Si + 5Zr + 4C$	26	$3 \times 3 \times 1$
2 × 2 slab C	$2Si + 11Zr + 10C$	30	$6 \times 6 \times 1$

^aModel A is a symmetric slab model for the structural optimization of the substrate. Model B is an asymmetric slab model used in the MD simulations, the bottom three layers of which are fixed at the bulk spacing. Model C is a symmetric slab for the phonon calculation.

to >2000 K in UHV. It exhibited a sharp 1 × 1 RHEED pattern and little impurity in the AES [Figure 1(a)]. ZrC was deposited

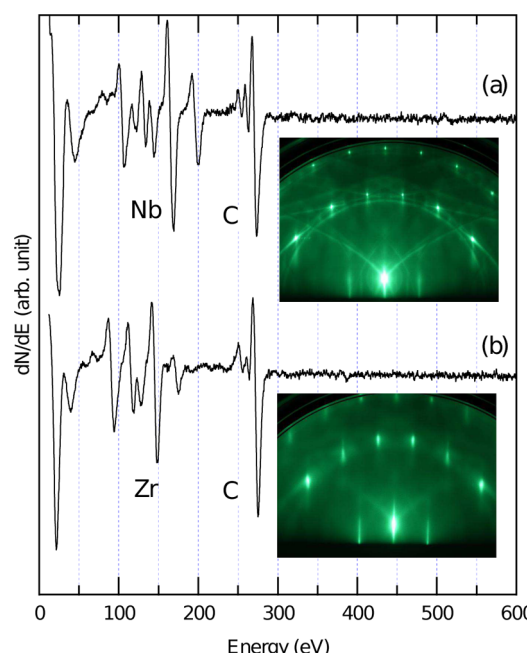


Figure 1. AES and RHEED patterns (inset) of (a) the clean NbC(111) surface and (b) epitaxially grown ZrC(111) film surface. The RHEED primary electron energy is 15 keV, and the azimuth is [1̄12].

onto the clean NbC(111) at a sample temperature of 1700 K. The grown ZrC film also exhibited a 1 × 1 RHEED pattern [Figure 1(b)], although the background was a little higher and the diffraction spot larger than those for NbC. The lattice constant of the film was estimated from the RHEED pattern at 328 pm, which agreed with that of ZrC(111) (332 pm) within the experimental error. The RHEED pattern indicated that the ZrC film had the same orientation as the substrate NbC, namely, a cube-on-cube epitaxial relationship of (111)_{ZrC} || (111)_{NbC} and [1̄10]_{ZrC} || [1̄10]_{NbC}. The slight contamination of O detected in the AES (not shown) just after the growth was easily removable with the subsequent flash heating above 1900 K. The clean ZrC(111) substrate was used in the following experiment.

ZrC Modeling. First, the ZrC bulk cell parameter was optimized. The optimization of a rock-salt-type ZrC bulk crystal provided a lattice parameter $a = 470.8$ pm and a bulk modulus of 214 GPa, which are very similar to the experimental values of 469.94 pm and 223.1 GPa, respectively, for ZrC_{0.94}.³⁸ The calculated bulk phonon dispersions [Figure 2(a)] were similar to those obtained in the previous calculations³⁹ and those obtained in neutron scattering experiments.

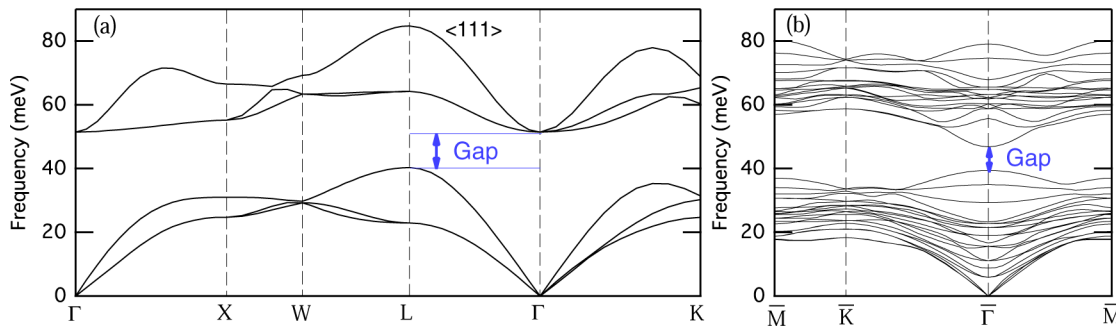


Figure 2. Calculated phonon dispersions for (a) ZrC bulk and (b) 13-layer ZrC(111) slab.

Second, the ZrC(111) surface was created, and the surface relaxation was performed. The surface relaxation was calculated using the 13-layer symmetric slab configuration (Slab A). In addition, an asymmetric slab consisting of six movable and three fixed layers was examined. The obtained surface relaxations listed in Table 2 agreed well with those of previous

calculation, the 13-layer slab was not sufficient to produce a gap suitable for silicene phonon appearance. Therefore, within our restricted computational resources, a slab thickness as high as possible is necessary for obtaining appropriate results.

■ SI OVERLAYER CHARACTERIZATION AND MODELING

Si Deposition. After flash heating for cleaning the surface, Si was deposited on the ZrC(111) at 800 K. The RHEED pattern changed from 1×1 to 2×2 in the first 30 s, and then it gradually diffused. When the 2×2 pattern was clearest (27 s), the deposition was stopped, and the sample was annealed at 1000–1100 K. Figure 3 shows the AES and RHEED of the as-

Table 2. Calculated Interlayer Spacing (pm) in the Vicinity of the ZrC(111) Surface

	d_{12}	d_{23}	d_{34}	d_{45}	d_{56}	d_{67}
PW ^a	111	152	128	140	133	136
ref ^b	111.7	151.3	129.9	137.8		

^aPresent work. ^bVojvodic et al.⁴⁰

calculations⁴⁰ and with the experimental value measured on HfC(111) ($d_{12} = 116$ pm).⁴¹ Note that the alternate relaxation expanded into considerably deep layers on this surface. These results confirmed the validity of our calculation condition.

Figure 2(b) shows the calculation result for the 13-layer slab model. Two phonon bands appeared separately: the lower-energy acoustic phonon band in which Zr has large amplitude, and the higher-energy optical phonon band in which mainly the C atoms vibrate. As per the projected bulk phonon dispersion along $\langle 111 \rangle$ ($\Gamma - L$), the band gap between the optical and the acoustic bands at the $\bar{\Gamma}$ point should be from 40.3 to 51.5 meV. However, the calculation in the slab model yielded a smaller gap (from 39.4 to 46.9 meV). The optical band minimum considerably dropped, even though, as per the eigenvector, the corresponding mode was not a surface mode. Table 3 shows the layer thickness dependency. The thicker the slab layer, the larger the band gap. In particular, the optical minimum frequency varied with the slab thickness. As described above, in the case of ZrC(111), surface formation introduced fairly large relaxation into several layers. The interatomic forces on C atoms may be considerably long-ranged. In the phonon

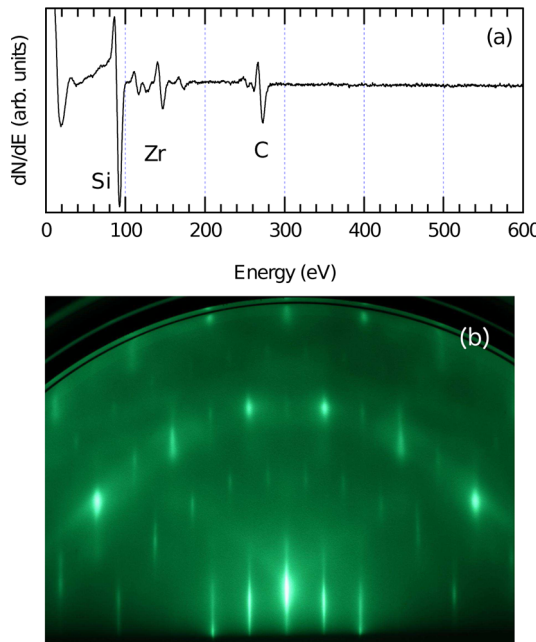


Figure 3. (a) AES and (b) RHEED pattern of Si on ZrC(111). RHEED primary electron energy is 15 keV, and the azimuth is $[1\bar{1}2]$.

Table 3. Calculated Phonon Band Gap (meV) at the $\bar{\Gamma}$ Point on ZrC(111) Slab Models^a

layer number	$F_{A\max}$	$F_{O\min}$	gap energy
13	39.4	46.9	7.4
17	39.7	47.4	7.8
21	39.5	48.3	8.8
25	39.8	49.0	9.2
∞^b	40.3	51.5	11.1

^aThe maximum acoustic band frequency $F_{A\max}$ and the minimum optical band $F_{O\min}$ are also listed. ^bFrom bulk phonon dispersion along $\langle 111 \rangle$.

prepared 2×2 sample. The Auger intensity ratio, Si LVV at 92 eV versus Zr MVV at 150 eV, was similar to that for a Si-saturated $ZrB_2(0001)2 \times 2$ surface. The 2×2 pattern reversibly changed to 1×1 at about 1000 K, which is discussed in the next section using molecular dynamics (MD) simulations. The surface Si lasted up to 1300 K, and the 2×2 phase reappeared after cooling.

Above 1500 K, Si overlayer desorption started, and a faint incommensurate RHEED pattern appeared. In the AES, the

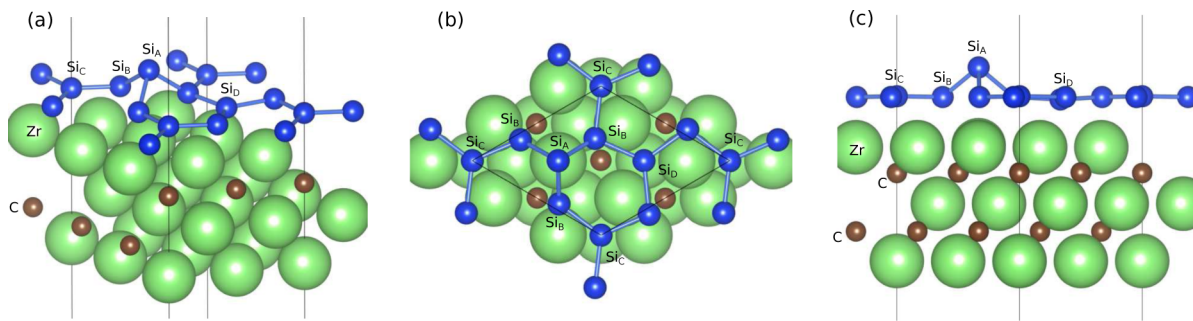


Figure 4. Optimized structure model of Si on ZrC(111). (a) Bird's eye, (b) planar, and (c) side views.

intensity of Si decreased to about 1/3 of that in the 2×2 phase. To remove Si completely, high-temperature flash heating at above 2300 K was necessary. After flash heating, a sharp 1×1 RHEED pattern recovered, and no Si was detected in the AES. The Si deposition experiments could be repeated on the same ZrC substrate.

The surface of the ZrC(111) substrate is chemically active similar to that of pure metals. For instance, it adsorbs $O_2^{42,43}$ and H_2^{44} dissociatively, and even in UHV (10^{-9} Pa), residual gas is gradually adsorbed. Once the surface is covered with silicene, it becomes dramatically inactive. After phonon measurements for over a month, any remarkable change was observed neither in the HREEL spectrum, in the AES, nor in the $2 \times 2 \leftrightarrow 1 \times 1$ phase transition temperature (1000 K) is slightly lower than that of the Si(111) $7 \times 7 \leftrightarrow 1 \times 1$ transition (1125 K).

In a preliminary experiment on Si/NbC(111), also a 2×2 structure was formed. However, the system was not stable compared to Si/ZrC(111). The HREELS exhibited several high frequency loss peaks above 100 meV on Si/NbC(111), which grew after 5 days in the vacuum, suggesting possible contamination adsorption. Moreover, that system was not stable upon heating. The RHEED exhibited complicated patterns after heating, thus indicating severe alloying of Si with the substrate. The carbon reduction observed in AES suggested the formation of Nb–Si compounds.

Si Overlayer Modeling. The AES Si/Zr ratio indicated that the Si coverage of ZrC(111) 2×2 -Si was similar to that of Si on ZrB₂(0001). We assumed the coverage of six Si atoms in the 2×2 unit cell of the ZrC(111) substrate in accordance with the proposed model for Si/ZrB₂(0001).

The structure optimization easily converged, resulting in a structure shown in Figure 4. In order to check whether this structure is stable or not, MD simulations (800 and 1200 K, 10 ps, 3 fs/MD-step) were performed. At 800 K, the atom vibrated around its position maintaining the structure. At 1200 K, the Si layer occasionally changed its registry, which means that the system can overcome some potential barriers. It agrees with the RHEED observation, in which the 2×2 periodicity was lost above 1000 K. However, even at 1200 K, the Si overlayer kept the main honeycomb framework. This result suggests that the phase transition to 1×1 at 1000 K does not correspond to the complete melting of the Si layer but to a loss of long-range ordering, thus indicating the order–disorder transition. After the system was cooled down, it returned to the same structure

as the initial one except for the registry. Note that the MD simulations also exhibited no tendency of Si alloying with Zr or C. From the MD simulations, we concluded that the proposed structure was the stable structure at this Si coverage.

In this structure model, one prominent Si atom (Si_A) was located on the on-top position of the substrate Zr. The three surrounding Si atoms (Si_B) were identical and were located at the bridge sites of the substrate. The other Si atoms were positioned at two different 3-fold hollow sites: one is above the third C layer (Si_C) and the other above the fourth Zr layer (Si_D). The height of Si atoms and the interlayer distances in the substrate are listed in Table 4. In the first Zr substrate layer,

Table 4. Calculated Si Heights (pm) from the First Zr Substrate Layer and Substrate Interlayer Spacings (d_{NN})

Si_A	Si_B	Si_C	Si_D	
374	239	239	224	
d_{12}	d_{23}	d_{34}	d_{45}	d_{56}
118	146	130	138	135
				136

only the Zr atom below Si_A was relaxed by 9 pm outward. Compared with the clean ZrC(111), the interlayer relaxation was slightly small but not largely affected by the Si adsorption. The interaction between Si and ZrC was not large enough to affect the substrate relaxation.

We have checked the effects of van der Waals (vdW) interaction using two functionals, PBE+D2⁴⁵ and rVV10.⁴⁶ The distance between Si_A and the Zr underneath (365 pm with PBE) contracted (358 pm, -1.9%) with the PBE+D2, but expanded (371 pm, +1.6%) with the rVV10 functional. The formation energy, namely, the energy difference between the 23-layers (2Si + 11Zr + 10C) and the clean ZrC slab (11Zr + 10C) plus bulk (diamond-type) Si, was calculated at -614 meV/Si atom in the PBE, at -677 meV/Si atom in the PBE+D2, and at -571 meV/Si atom in the rVV10. In contrast to graphene on Ni,^{47,48} this system was stable even without the vdW interaction. Anyway, as the vdW effects were not critical either in structure or in energy, it was not taken into account in the following calculations. In fact, the shortest nearest-neighbor Si–Zr distance in our model is 273 pm between Si_B and the Zr below, which is comparable with the Si–Zr distance in zirconium disilicide ZrSi₂, 267 pm.⁴⁹ The interaction between silicene and substrate might be considerably covalent or metallic.

The structure model exhibited a characteristic distortion in the $\sqrt{3} \times \sqrt{3}$ cell of silicene. One Si atom in the unit cell protruded from the other flat Si layer. This type of silicene ($\sqrt{3}$ -silicene, hereafter) has been commonly proposed in

$\text{ZrB}_2(0001)2 \times 2\text{-Si}$,⁵⁰ $\text{Ir}(111)\sqrt{7} \times \sqrt{7}\text{-Si}$,¹⁸ and Si on $\text{Ag}(111)$.⁵¹ However, in the case of Si/ ZrB_2 , relatively large compression stress in silicene may cause an incommensurate layer with the substrate. Considering the stripe domains observed in the STM,¹⁹ the silicene may coincide anisotropically with the substrate, making a complicated domain structure. In the case of Si/Ir, the suspicion of alloying in the surface layer has been recently discussed.⁵² On $\text{Ag}(111)$, several $\sqrt{3}$ -silicene phases coexisted, and it was difficult to obtain a single phase in single domains.⁵¹ In the structure model of $\sqrt{3}$ -silicene/ $\text{Ag}(111)$, the registry of the prominent Si varies with each unit cell, suggesting weak interactions between the Si layer and the Ag substrate. Conversely, the $\sqrt{3}$ -silicene fitted to the 2×2 $\text{ZrC}(111)$, making a commensurate structure. At saturation coverage, the single-domain single-phase structure was very easily obtained. Therefore, this system could be a clean prototype of $\sqrt{3}$ -silicene.

Phonon Dispersion. The HREELS measurements were performed on the $\text{ZrC}(111)2 \times 2\text{-Si}$. Figure 5 shows a typical

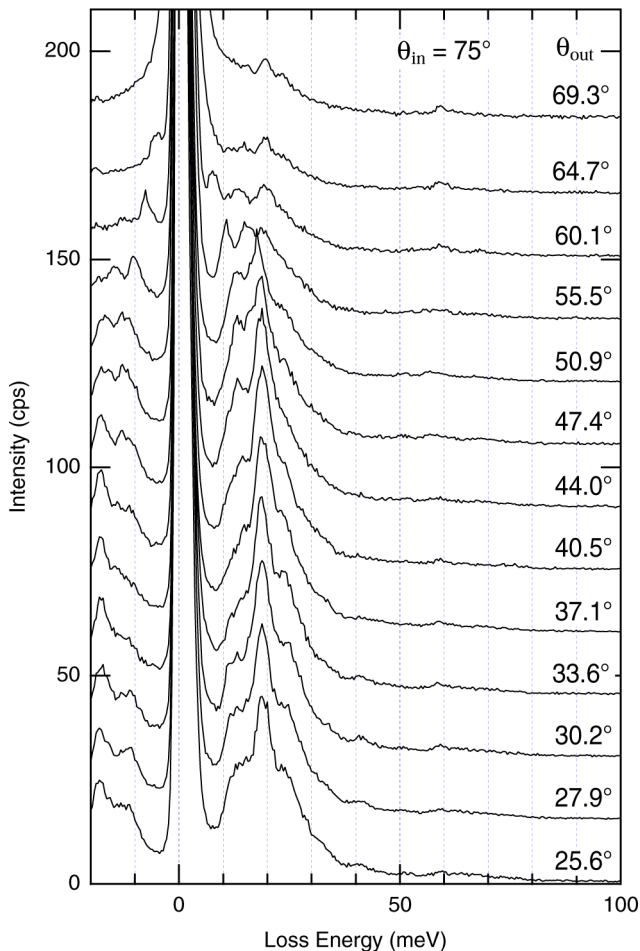


Figure 5. Series of HREEL spectra for Si on $\text{ZrC}(111)$. The azimuth along $\bar{\Gamma} - \bar{K} - \bar{M}$ in the surface Brillouin zone is $[1\bar{1}0]$. E_0 is 26 eV.

series of off-specular HREEL spectra. As per the detection angle θ_{out} , some loss peaks changed their energies. We adopted several primary energies E_0 in the HREELS to detect as many phonon modes as possible. The obtained phonon dispersion relations are presented in Figure 6. Except for the acoustic surface phonon near $\bar{\Gamma}$ in the low-energy region, the observed

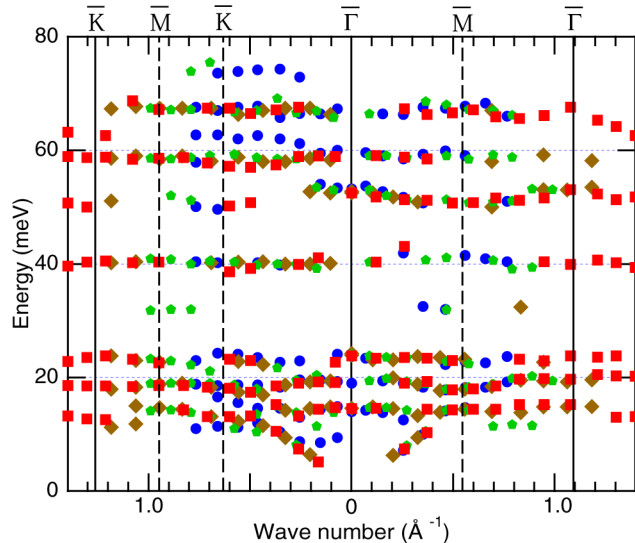


Figure 6. Measured phonon dispersion relations of Si on $\text{ZrC}(111)$. The primary electron energies (E_0) are 9 eV (blue circles), 14 eV (green pentagons), 20 eV (brown diamonds), and 26 eV (red squares).

dispersion was small, indicating that the atomic bond within the overlayer was not as strong as that in a graphene layer.

From the measured phonon dispersion relations, no anomalous softening was observed at the $\bar{\Gamma}$ point within the experimental sensitivity. In the case of graphene, Kohn anomalies are observed at the $\bar{\Gamma}$ and \bar{K} points.^{53–55} In the $\sqrt{3} \times \sqrt{3}$ periodicity, the \bar{K} point is folded back to the $\bar{\Gamma}$ point. Therefore, the Kohn anomaly should be observed at the $\bar{\Gamma}$ point if it existed. Probably the large mixing of the silicene electronic state with the substrate breaks the possible anomalies of the silicene phonons.

The calculated phonon dispersions of a thicker 23-layer (2Si, 11Zr, and 10C) slab are shown in Figure 7(a). The phonon partial density of state (PDOS) was calculated for the Si surface layer and compared with the experimental values [Figure 7(b)–(d)]. The Si phonon modes can be classified into two: lower frequency (<30 meV) Si–Zr vibrations and higher frequency (40–60 meV) Si–Si vibrations. If Si were atomically adsorbed on the ZrC surface, no Si–Si vibration would be observed. The Si–Si bond is basically surface parallel in a silicene layer; the latter high frequency modes correspond to longitudinal or shear-horizontal ones and the former low frequency modes to vertical ones.

Compared with the experimental data, the modes above 55 meV and around 25 meV correspond with the dense DOS regions in the calculated bulk band, as shown in Figure 7(a). The low-energy mode around 20 meV, the 10–15 meV mode, and largely dispersed acoustic surface mode are reproduced well in the calculated Si vertical vibrating PDOS shown in Figure 7(b). Within the Si–Si frequency range, the 52 meV mode exceptionally has some vertical component around $\bar{\Gamma}$. As discussed below, this is the localized mode at the prominent Si atom. Among the other observed Si vibrational modes parallel to the surface, the mode around 40 meV agrees well with the calculation, but the mode around 52 meV is at slightly lower values in the calculation than in the experiment. This probably arises from the resonance with the slab optical phonon. As discussed in the ZrC slab construction, the calculated optical band minimum largely depends on the slab thickness. In

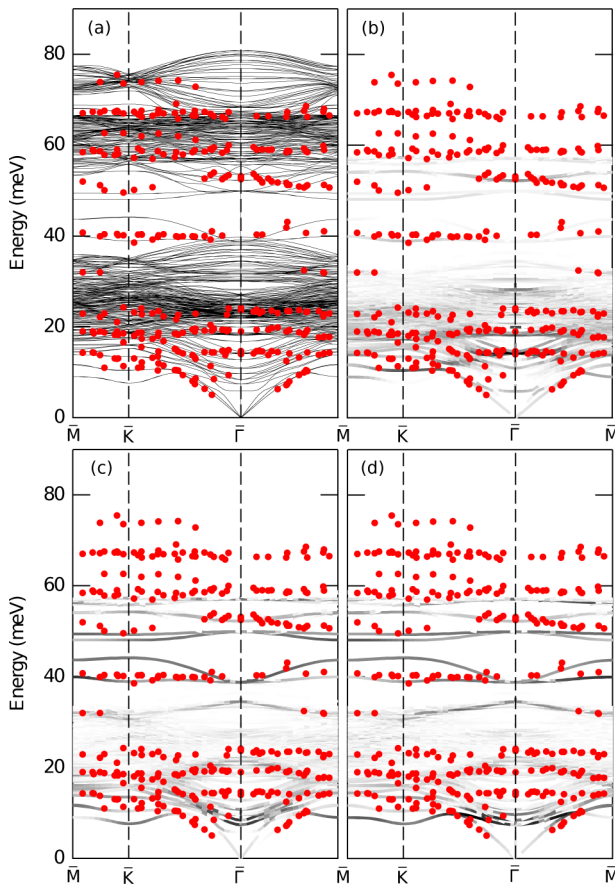


Figure 7. Comparison between the calculated phonon dispersion relations for the 2×2 Si on ZrC(111) slab (black lines) and the experimental data (red dots). All phonon modes (a) and PDOS for the vertical (b), longitudinal (c), and shear horizontal (d) components on the surface Si vibrations are exhibited.

another calculation where the bottom of the slab was fixed (as in the asymmetric model B), this mode agrees well with the experiment. In this case, the bulk phonon band is not reproduced at all, and the bulk optical band minimum is much higher (~ 60 meV). Specifically, if the interaction with the bulk optical band were weak, the calculated mode should be similar to the experiment. As the bulk band minimum gradually increases with the slab thickness, the deviation would diminish in calculations with the thicker slab model. The 23-layer slab was not thick enough to provide accurate reproduction of this phonon.

In Figure 8, the specular HREEL spectrum is compared with the vertical vibration PDOS of the Si overlayer at the $\bar{\Gamma}$ point. Since the absolute intensity of the loss peak is about 1 order of magnitude larger than that in the off-specular HREELS, the observed loss features correspond to dipole-active phonon modes, which have a large vertical component. As shown in Figure 8, five noticeable peaks (A–F) emerged from the calculations. Within these peaks, A–C and E have their corresponding structures in the experimental spectrum. The frequency range of A–C corresponds with the Si–Zr vertical vibrations. The peak E frequency is within the Si–Si vibration range. If the silicene layer were flat or little buckled, any Si–Si vibration could not be dipole active. The eigenvectors of mode E are shown in the inset. The on-top Si_A vibrates vertically, and the three surrounding Si_B atoms have vertical amplitude in the

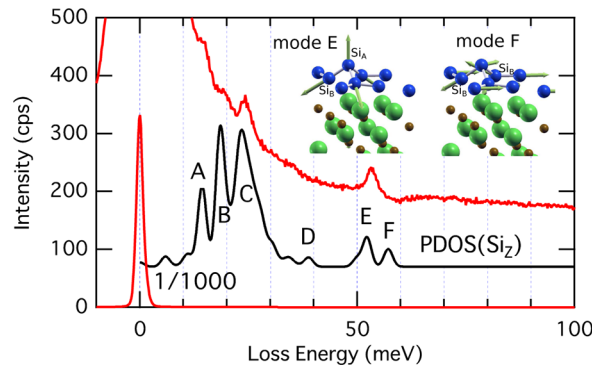


Figure 8. Specular HREELS ($E_0 = 9$ eV) of the Si on ZrC(111) (red line) and calculated PDOS of the vertical vibrations of Si at $\bar{\Gamma}$. The calculated PDOS is broadened with a Gaussian of 1 meV width to simulate the experimental spectrum and is arbitrarily magnified for comparison.

opposite phase. Because the chemical status and the charge of Si_A and Si_B are different from each other, this mode can be dipole active. The dipole-active Si–Si vibration clearly indicates the existence of a prominent Si atom.

The modes D and F are not observed in the specular HREELS. In the mode F, the two Si_B atoms have the vertical component in the opposite direction. These Si_B atoms are chemically identical in the unit cell and are equally charged. The out-of-phase vertical components compensate the dipole to zero. Similarly, mode D is also dipole inactive. All dipole-active phonon modes observed in the specular HREELS have been associated with the Si vertical vibration components in the silicene layer. Considering that the calculation did not employ empirical parameters, this agreement appears excellent.

We also calculated the substitution of one Si with C in the $\sqrt{3}$ -silicene. The most stable site was the Si_A (on-top) site, where a high frequency vibrational mode of C appeared at 95.6–96.0 meV that is not observed in the experiment. C contamination in the $\sqrt{3}$ -silicene can be excluded.

Calculated Electronic Structure. Figure 9 is the calculated electronic band structure for our model in the symmetric 23-layer slab. In addition to the total electronic band structure, PDOSs of the surface Si, of the subsurface Zr, and of the third layer C are calculated. Between Zr and C, strong mixed bands exist around -3 eV (Zr 4d and C 2p) and around -10 eV (Zr 5s, 5p, and C 2s), indicating strong covalent bonding. In the Si PDOS, the original σ band feature is preserved in the substrate gap region (from -5 to -8 eV). Above -5 eV, Si and Zr bands are mixed. At the $\bar{\Gamma}$ point, where the \bar{K} point of 1×1 silicene is folded back in the $\sqrt{3} \times \sqrt{3}$ periodicity, no crossing of the π band is observed on the Fermi level, suggesting that the expected Dirac cone^{22,56} is lost. Instead, mixed bands consisting of the Zr 4d and Si 3p appear at about -0.3 , -1.2 , $+1.9$, and $+3.3$ eV, suggesting considerable covalent nature. Figure 10 shows the calculated valence charge density of the proposed model. Between Si atoms a typical covalent bond can be recognized. Additionally, between the Si_B and the subsurface Zr, a small neck is seen, suggesting a little covalency.

CONCLUSION

Si deposition on a ZrC(111) film substrate resulted in an ordered silicene layer with 2×2 substrate periodicity, which coincided with the $\sqrt{3} \times \sqrt{3}$ cell of silicene. The phonon dispersion relations of Si/ZrC(111) were measured using

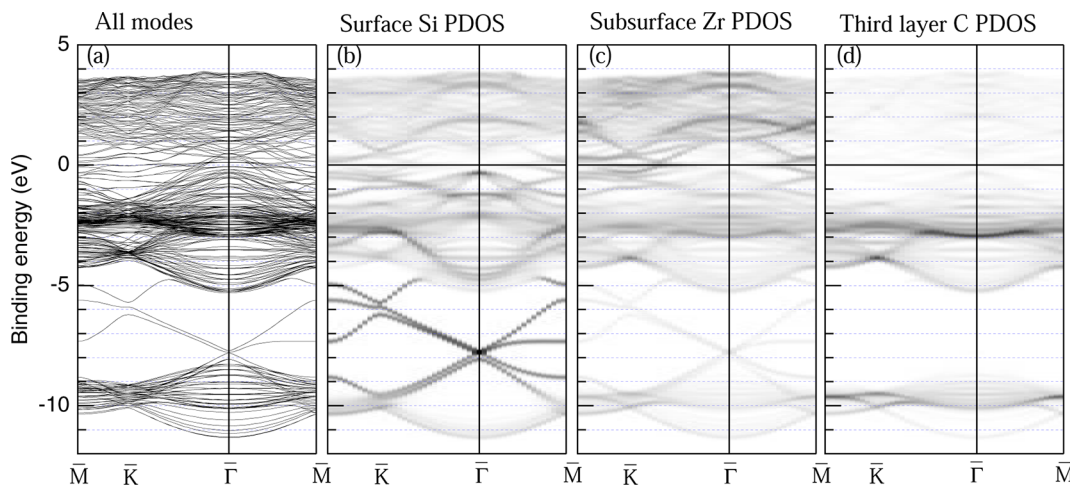


Figure 9. Calculated electronic bands for the 23-layer ZrC(111)2 × 2-Si slab. (a) All the slab bands, (b) PDOS of the surface Si, (c) PDOS of the subsurface Zr, and (d) PDOS of the third layer C.

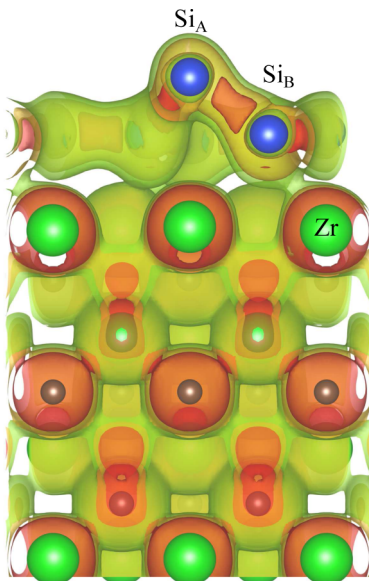


Figure 10. Calculated valence charge density for ZrC(111)2 × 2-Si. The front face is a (11̄2) section including Si_A and Si_B.

HREELS. The observed phonon indicates (a) the existence of Si–Si covalent bonded network and (b) the existence of (at least) one prominent Si from the other flat layers. The ab initio DFT calculations predicted a distorted silicene structure, which agrees with the above-mentioned criteria. The calculated phonon dispersion agreed well with the experiment, even though not all the calculated modes were observed experimentally. Especially, the dipole-active spectrum measured in the specular HREELS condition agreed well with the calculation, verifying the proposed structure. The silicene-covered surface was relatively inert to gas adsorption and stable upon heating up to 1300 K, while order–disorder phase transition occurred at approximately 1000 K. This system is a clear example of a $\sqrt{3} \times \sqrt{3}$ distorted silicene.

AUTHOR INFORMATION

Corresponding Author

*E-mail: aizawa.takashi@nims.go.jp.

Notes

The authors declare no competing financial interest.

ACKNOWLEDGMENTS

This study was partly supported by JSPS KAKENHI Grant Number 24560035.

REFERENCES

- (1) Kara, A.; Enriquez, H.; Seitsonen, A. P.; Voon, L. C. L. Y.; Vizzini, S.; Aufrayg, B.; Oughaddou, H. A review on silicene — New candidate for electronics. *Surf. Sci. Rep.* **2012**, *67*, 1.
- (2) Vogt, P.; Padova, P. D.; Quaresima, C.; Avila, J.; Frantzeskakis, E.; Asensio, M. C.; Resta, A.; Ealet, B.; Lay, G. L. Silicene: Compelling Experimental Evidence for Graphenelike Two-Dimensional Silicon. *Phys. Rev. Lett.* **2012**, *108*, 155501.
- (3) Jamgotchian, H.; Colignon, Y.; Hamzaoui, N.; Ealet, B.; Hoarau, J. Y.; Aufray, B.; Bibérian, J. P. Growth of silicene layers on Ag(111): unexpected effect of the substrate temperature. *J. Phys.: Condens. Matter* **2012**, *24*, 172001.
- (4) Lay, G. L.; Padova, P. D.; Resta, A.; Bruhn, T.; Vogt, P. Epitaxial silicene: can it be strongly strained? *J. Phys. D: Appl. Phys.* **2012**, *45*, 392001.
- (5) Enriquez, H.; Vizzini, S.; Kara, A.; Lalm, B.; Oughaddou, H. Silicene structures on silver surfaces. *J. Phys.: Condens. Matter* **2012**, *24*, 314211.
- (6) Arafune, R.; Lin, C.-L.; Kawahara, K.; Tsukahara, N.; Minamitani, E.; Kim, Y.; Takagi, N.; Kawai, M. Structural transition of silicene on Ag(111). *Surf. Sci.* **2013**, *608*, 297.
- (7) Majzik, Z.; Tchalala, M. R.; Švec, M.; Hapala, P.; Enriquez, H.; Kara, A.; Mayne, A. J.; Dujardin, G.; Jelnek, P.; Oughaddou, H. Combined AFM and STM measurements of a silicene sheet grown on the Ag(111) surface. *J. Phys.: Condens. Matter* **2013**, *25*, 225301.
- (8) Fukaya, Y.; Mochizuki, I.; Maekawa, M.; Wada, K.; Hyodo, T.; Matsuda, I.; Kawasuso, A. Structure of silicene on a Ag(111) surface studied by reflection high-energy positron diffraction. *Phys. Rev. B* **2013**, *88*, 205413.
- (9) Kawahara, K.; Shirasawa, T.; Arafune, R.; Lin, C.-L.; Takahashi, T.; Kawai, M.; Takagi, N. Determination of atomic positions in silicene on Ag(111) by low-energy electron diffraction. *Surf. Sci.* **2014**, *623*, 25.
- (10) Avila, J.; Padova, P. D.; Cho, S.; Colombo, I.; Lorcy, S.; Quaresima, C.; Vogt, P.; Resta, A.; Lay, G. L.; Asensio, M. C. Presence of gapped silicene-derived band in the prototypical (3 × 3) silicene phase on silver (111) surfaces. *J. Phys.: Condens. Matter* **2013**, *25*, 262001.
- (11) Padova, P. D.; Vogt, P.; Resta, A.; Avila, J.; Razado-Colombo, I.; Quaresima, C.; Ottaviani, C.; Olivieri, B.; Bruhn, T.; Hirahara, T.; et al.

- Evidence of Dirac fermions in multilayer silicene. *Appl. Phys. Lett.* **2013**, *102*, 163106.
- (12) Padova, P. D.; Avila, J.; Resta, A.; Razado-Colombo, I.; Quaresima, C.; Ottaviani, C.; Olivieri, B.; Bruhn, T.; Vogt, P.; Asensio, M. C.; et al. The quasiparticle band dispersion in epitaxial multilayer silicene. *J. Phys.: Condens. Matter* **2013**, *25*, 382202.
- (13) Gori, P.; Pulci, O.; Ronci, F.; Colonna, S.; Bechstedt, F. Origin of Dirac-cone-like features in silicon structures on Ag(111) and Ag(110). *J. Appl. Phys.* **2013**, *114*, 113710.
- (14) Tsoutsou, D.; Xenogianopoulos, E.; Golias, E.; Tsipas, P.; Dimoulas, A. Evidence for hybrid surface metallic band in (4 × 4) silicene on Ag(111). *Appl. Phys. Lett.* **2013**, *103*, 231604.
- (15) Cinquanta, E.; Scalise, E.; Chiappe, D.; Grazianetti, C.; van den Broek, B.; Houssa, M.; Fanciulli, M.; Molle, A. Getting through the Nature of Silicene: An sp^2 – sp^3 Two-Dimensional Silicon Nanosheet. *J. Phys. Chem. C* **2013**, *117*, 16719.
- (16) Ding, Y.; Wang, Y. Density Functional Theory Study of the Silicene-like SiX and XSi₃ (X = B, C, N, Al, P) Honeycomb Lattices: The Various Buckled Structures and Versatile Electronic Properties. *J. Phys. Chem. C* **2013**, *117*, 18266.
- (17) Scalise, E.; Cinquanta, E.; Houssa, M.; van den Broek, B.; Chiappe, D.; Grazianetti, C.; Pourtois, G.; Ealet, B.; Molle, A.; Fanciulli, M.; et al. Vibrational properties of epitaxial silicene layers on (111) Ag. *Appl. Surf. Sci.* **2014**, *291*, 113.
- (18) Meng, L.; Wang, Y.; Zhang, L.; Du, S.; Wu, R.; Li, L.; Zhang, Y.; Li, G.; Zhou, H.; Hofer, W. A.; et al. Buckled Silicene Formation on Ir(111). *Nano Lett.* **2013**, *13*, 685.
- (19) Fleurence, A.; Friedlein, R.; Ozaki, T.; Kawai, H.; Wang, Y.; Yamada-Takamura, Y. Experimental Evidence for Epitaxial Silicene on Diboride Thin Films. *Phys. Rev. Lett.* **2012**, *108*, 245501.
- (20) Aizawa, T.; Souda, R.; Otani, S.; Ishizawa, Y.; Oshima, C. Anomalous Bond of Monolayer Graphite on Transition-Metal Carbide Surfaces. *Phys. Rev. Lett.* **1990**, *64*, 768.
- (21) Aizawa, T.; Souda, R.; Otani, S.; Ishizawa, Y.; Oshima, C. Bond softening in monolayer graphite formed on transition-metal carbide surfaces. *Phys. Rev. B* **1990**, *42*, 11469.
- (22) Cahangirov, S.; Topsakal, M.; Aktürk, E.; Şahin, H.; Ciraci, S. Two- and One-Dimensional Honeycomb Structures of Silicon and Germanium. *Phys. Rev. Lett.* **2009**, *102*, 236804.
- (23) Cheng, Y. C.; Zhu, Z. Y.; Schwingenschlögl, U. Doped silicene: Evidence of a wide stability range. *Europhys. Lett.* **2011**, *95*, 17005.
- (24) Pan, L.; Liu, H. J.; Wen, Y. W.; Tan, X. J.; Lv, H. Y.; Shi, J.; Tang, X. F. First-principles study of monolayer and bilayer honeycomb structures of group-IV elements and their binary compounds. *Phys. Lett. A* **2011**, *375*, 614.
- (25) Scalise, E.; Houssa, M.; Pourtois, G.; van den Broek, B.; Afanásiev, V.; Stesmans, A. Vibrational properties of silicene and germanene. *Nano Res.* **2013**, *6*, 19.
- (26) Kinoshita, H.; Otani, S.; Kamiyama, S.; Amano, H.; Akasaki, I.; Suda, J.; Matsunami, H. Zirconium Diboride (0001) as an Electrically Conductive Lattice-Matched Substrate for Gallium Nitride. *Jpn. J. Appl. Phys.* **2001**, *40*, L1280.
- (27) Kinoshita, H.; Otani, S.; Kamiyama, S.; Amano, H.; Akasaki, I.; Suda, J.; Matsunami, H. ZrB₂ Substrate for Nitride Semiconductors. *Jpn. J. Appl. Phys.* **2003**, *42*, 2260.
- (28) Tomida, Y.; Nitta, S.; Kamiyama, S.; Amano, H.; Akasaki, I.; Otani, S.; Kinoshita, H.; Liu, R.; Bell, A.; Ponce, F. A. Growth of GaN on ZrB₂ substrate by metal-organic vapor phase epitaxy. *Appl. Surf. Sci.* **2003**, *216*, 502.
- (29) Aizawa, T.; Hishita, S.; Otani, S. Plasma-assisted molecular-beam epitaxy of GaN on transition-metal carbide (111) surfaces. *J. Cryst. Growth* **2008**, *310*, 22.
- (30) Friedlein, R.; Fleurence, A.; Sadowski, J. T.; Yamada-Takamura, Y. Tuning of silicene-substrate interactions with potassium adsorption. *Appl. Phys. Lett.* **2013**, *102*, 221603.
- (31) Ibach, H.; Mills, D. L. *Electron Energy Loss Spectroscopy and Surface Vibrations*; Academic Press: New York, 1982.
- (32) Giannozzi, P.; Baroni, S.; Bonini, N.; Calandra, M.; Car, R.; Cavazzoni, C.; Ceresoli, D.; Chiarotti, G. L.; Cococcioni, M.; Dabo, I.; et al. QUANTUM ESPRESSO: a modular and open-source software project for quantum simulations of materials. *J. Phys.: Condens. Matter* **2009**, *21*, 395502.
- (33) Perdew, J. P.; Burke, K.; Ernzerhof, M. Generalized Gradient Approximation Made Simple. *Phys. Rev. Lett.* **1996**, *77*, 3865.
- (34) Garrity, K. F.; Bennett, J. W.; Rabe, K. M.; Vanderbilt, D. Pseudopotentials for high-throughput DFT calculations. *Comput. Mater. Sci.* **2014**, *81*, 446.
- (35) Baroni, S.; de Gironcoli, S.; Corso, A. D.; Giannozzi, P. Phonons and related crystal properties from density-functional perturbation theory. *Rev. Mod. Phys.* **2001**, *73*, 515.
- (36) Kokalj, A. Computer graphics and graphical user interfaces as tools in simulations of matter at the atomic scale. *Comput. Mater. Sci.* **2003**, *28*, 155.
- (37) Momma, K.; Izumi, F. VESTA: a three-dimensional visualization system for electronic and structural analysis. *J. Appl. Crystallogr.* **2008**, *41*, 653.
- (38) Chang, R.; Graham, L. J. Low-Temperature Elastic Properties of ZrC and TiC. *J. Appl. Phys.* **1966**, *37*.
- (39) Jochym, P. T.; Parlinski, K. Ab initio lattice dynamics and elastic constants of ZrC. *Eur. Phys. J. B* **2000**, *15*, 265.
- (40) Vojvodic, A.; Ruberto, C.; Lundqvist, B. I. Atomic and molecular adsorption on transition-metal carbide (111) surfaces from density-functional theory: a trend study of surface electronic factors. *J. Phys.: Condens. Matter* **2010**, *22*, 375504.
- (41) Hayami, W.; Souda, R.; Aizawa, T.; Otani, S.; Ishizawa, Y. Analysis of the HfC(111) surface structure by impact collision ion scattering spectroscopy (ICISS). *Surf. Sci.* **1992**, *276*, 299.
- (42) Noda, T.; Nakane, T.; Ozawa, K.; Edamoto, K.; Tanaka, S.; Otani, S. Photoemission study of the oxidation of ZrC(111). *Solid State Commun.* **1998**, *107*, 145.
- (43) Noda, T.; Yamazaki, M.; Ozawa, K.; Edamoto, K.; Otani, S. Oxygen adsorption on a ZrC(111) surface: angle-resolved photoemission study. *Surf. Sci.* **2000**, *450*, 27.
- (44) Aizawa, T.; Hayami, W.; Souda, R.; Otani, S.; Ishizawa, Y. Hydrogen adsorption on transition-metal carbide (111) surfaces. *Surf. Sci.* **1997**, *381*, 157.
- (45) Grimme, S. Semiempirical GGA-type density functional constructed with a long-range dispersion correction. *J. Comput. Chem.* **2006**, *27*, 1787.
- (46) Sabatini, R.; Gorni, T.; de Gironcoli, S. Nonlocal van der Waals density functional made simple and efficient. *Phys. Rev. B* **2013**, *87*, 041108(R).
- (47) Vanin, M.; Mortensen, J. J.; Kelkkanen, A. K.; Garcia-Lastra, J. M.; Thygesen, K. S.; Jacobsen, K. W. Graphene on metals: A van der Waals density functional study. *Phys. Rev. B* **2010**, *81*, 081408(R).
- (48) Zhang, W.-B.; Chen, C.; Tang, P.-Y. First-principles study for stability and binding mechanism of graphene/Ni(111) interface: Role of vdW interaction. *J. Chem. Phys.* **2014**, *141*, 044708.
- (49) Zatorska, G. M.; Dmytriv, G. S.; Pavlyuk, V. V.; Bartzokas, A.; Jaskolski, M. Crystal structure of the new intermetallic compound $Zr_{2-x}Li_{x+y}Si_{1-y}$ ($x = 0.17$, $y = 0.12$) and its relation with the disilicide $ZrSi_2$. *J. Alloys Compd.* **2002**, *346*, 154.
- (50) Lee, C.-C.; Fleurence, A.; Friedlein, R.; Yamada-Takamura, Y.; Ozaki, T. First-principles study on competing phases of silicene: Effect of substrate and strain. *Phys. Rev. B* **2013**, *88*, 165404.
- (51) Chen, L.; Li, H.; Feng, B.; Ding, Z.; Qiu, J.; Cheng, P.; Wu, K.; Meng, S. Spontaneous Symmetry Breaking and Dynamic Phase Transition in Monolayer Silicene. *Phys. Rev. Lett.* **2013**, *110*, 085504.
- (52) Švec, M.; Hapala, P.; Ondráček, M.; Merino, P.; Blanco-Rey, M.; Mutombo, P.; Vondráček, M.; Polyak, Y.; Cháb, V.; Gago, J. A. M.; et al. Silicene vs. 2D ordered silicide: the atomic and electronic structure of the Si-($\sqrt{19} \times \sqrt{19}$)R23.4°/Pt(111). *Phys. Rev. B* **2014**, *89*, 201412(R).
- (53) Piscanec, S.; Lazzeri, M.; Mauri, F.; Ferrari, A. C.; Robertson, J. Kohn Anomalies and Electron-Phonon Interactions in Graphite. *Phys. Rev. Lett.* **2004**, *93*, 185503.
- (54) Yanagisawa, H.; Tanaka, T.; Ishida, Y.; Matsue, M.; Rokuta, E.; Otani, S.; Oshima, C. Analysis of phonons in graphene sheets by

means of HREELS measurement and ab initio calculation. *Surf. Interface Anal.* **2005**, *37*, 133.

(55) Politano, A.; Marino, A. R.; Formoso, V.; Chiarello, G. Evidence of Kohn anomalies in quasi-freestanding graphene on Pt(111). *Carbon* **2012**, *50*, 734.

(56) Takeda, K.; Shiraishi, K. Theoretical possibility of stage corrugation in Si and Ge analogs of graphite. *Phys. Rev. B* **1994**, *50*, 14916.